Article

Submarine maneuvering performance analysis: a study of the effect of different rudder angle settings on the turning dynamics of SUBOFF submarine

Guanyixuan Zhao[1], Yining Zhang[1,*], Yifan Xie[1],Zhenjie Liang[1],Qifeng Lin[1],Haoyu Jiang[2]

[1] Ship and Maritime College, Guangdong Ocean University, Zhanjiang 524005 China
[2] School of Electronics and Information Engineering, Guangdong Ocean University, Zhanjiang 316021, China
Academic Editor: Dapeng Zhang <zhangdapeng@gdou.edu.cn>

Abstract: In the ongoing pursuit of bolstering maritime military capabilities, the optimization and augmentation of submarine performance stand as pivotal objectives within the realm of strategic naval power. Given the exacting operational standards required for submarines to execute vital missions like reconnaissance, stealthy attacks, and tracking, this study leverages Computational Fluid Dynamics (CFD) simulation technology to meticulously analyze and evaluate submarine maneuverability under various rudder angle configurations. Through a thorough examination of a spectrum of simulation results, this study unveils the critical determinants influencing submarine maneuverability and proposes corresponding optimization strategies. The outcomes not only furnish a robust scientific foundation for enhancing submarine maneuvering capabilities but also offer valuable technical insights for advancing overall submarine operational efficacy. The discoveries of this study bear significant practical significance and applicability, guiding submarine design endeavors and fortifying tactical responsiveness in intricate maritime settings.

Eng. Solut. Mech. Mar. Struct. Infrastruct., 2024, Vol. 1. Issue 2

2 of 22

1. Introduction

Amidst the relentless advancement of global military technologies, a nation's military prowess stands as a pivotal determinant of its position on the international stage. With approximately 71% of the Earth's surface covered by oceans and China boasting an extensive territorial sea area, the cultivation of maritime military capabilities emerges as paramount for national security [1]. Among the array of maritime military assets, submarines hold an indispensable role in modern naval warfare owing to their unparalleled stealth and versatility [2]. Submarines undertake a spectrum of missions, encompassing reconnaissance, surveillance, anti-submarine warfare, and ground attack, with the success of these endeavors hinging heavily upon the mobility and stealthiness of these vessels [3].Nonetheless, extant submarines confront performance limitations during turning operations, characterized by phenomena such as velocity drop and wake divergence, which impede maneuverability and stealthiness [4]. The rudder angle emerges as a pivotal parameter influencing submarine turning performance, underscoring the significance of optimizing this variable to enhance tactical responsiveness and survivability. As Computational Fluid Dynamics (CFD) technology matures and gains widespread adoption across various fields [5], its application in ocean engineering becomes increasingly sophisticated [6-8]. In this paper, we utilize CFD software to simulate the flow field around a submarine during its rotation. By analyzing these simulation results, we can identify challenges encountered during submarine maneuvers. Subsequently, leveraging these findings, we propose modifications and upgrades to enhance the submarine's performance and operational effectiveness.

Liu Qinxian et al. formulated a comprehensive set of equations of motion for submarines, utilizing computer simulations to elucidate the correlation between the submarine's rudder angle and the radius of gyration [9]. He Guangxing et al. conducted numerical simulations to investigate parameters such as gyration period at varying speeds [10]. In addition, Li S. Q. Q. et al. conducted a comparative analysis of transverse rudder and X rudder submarines and found that the X rudder configuration outperformed the transverse rudder configuration in terms of manoeuvre performance [11].

To delve deeper into the influence of rudder angle on submarine turning performance, we conduct a meticulous analysis of the underlying physical mechanisms governing submarine maneuverability across various rudder angle configurations using simulation. Through this approach, we aim to unravel the intricacies of submarine turning dynamics and pinpoint shortcomings in existing submarine designs during turning maneuvers.

This paper commences by outlining the equations of motion governing submarine dynamics and introduces the concept of the self-propelled point. Subsequently, employing Computational Fluid Dynamics (CFD), turning simulations are conducted[12], followed by a comprehensive analysis of the simulation outcomes. Finally, the paper suggests some improvements for the experimental results. The mind map for this paper is shown in Figure 1.The primary objective of this study is to establish a quantitative correlation between rudder angle and submarine turning performance, aiming to propose enhancement measures to bolster turning capabilities. Through an exhaustive examination of CFD simulation results,

the paper scrutinizes submarine turning deficiencies, offering targeted improvement recommendations. The research outcomes not only furnish a theoretical framework for submarine design but also furnish scientific insights to inform the formulation of submarine maneuvering strategies, thereby possessing both theoretical and practical significance.
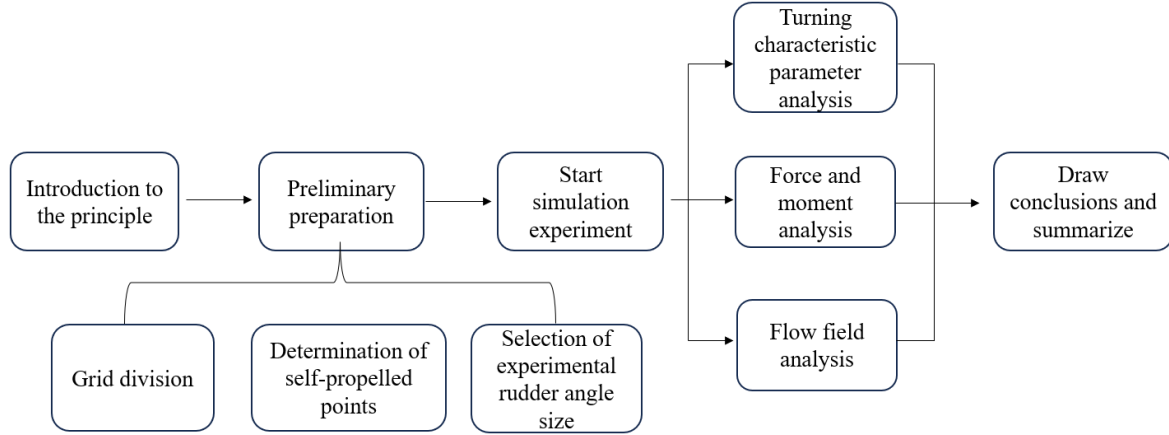
Figure. 1. Mind map for this article

2. Equations of motion for a submarine

The data obtained in the experiment need to be processed using the formula, especially the submarine underwater along the length direction of the force complexity of various coupling is more obvious, a suitable equation is particularly important. After considering the submarine underwater force characteristics according to reference [13], combined with the submarine underwater constant turning motion steady state conditions:

$$\dot{u} = \dot{v} = \dot{w} = \dot{p} = \dot{q} = \dot{r} = \dot{\phi} = \dot{\theta} = 0; \dot{\psi} = C(\text{a constant}) \tag{1}$$

Simplification to a constant differential form yields:

$$f(x,\mu) = (f_1(x,\mu), f_2(x,\mu), \cdots, f_9(x,\mu)) = 0 \tag{2}$$

Includes:

$$f_1(x,\mu) = \frac{\rho}{2}L^4[X_{pp}p^2 + X_{qq}q^2 + X_{rr}r^2 + X_{pr}pr] + \frac{\rho}{2}L^3[X_{wq}wq + X_{vp}vp + X_{vr}vr +$$

$$up(X_{q\delta s}\delta_s + X_{q\delta b}\delta_b) + X_{r\delta r}ur\delta_r] + \frac{\rho}{2}L^2[X_{vv}v^2 + X_{ww}w^2 + X_{v\delta r}uv\delta_r + uw(X_{v\delta s}\delta_s + \tag{3}$$

$$X_{w\delta b}\delta_b) + u^2(X_{\delta s\delta s}\delta_s^2 + X_{\delta b\delta b}\delta_b^2 + X_{\delta r\delta r}\delta_r^2 + X_{prop})] -$$

$$m[-vr + wq - x_G(q^2 + r^2) + y_G pq + z_G pr] - (W - B)\sin\theta$$

$$f_2(x,\mu) = \frac{\rho}{2}L^4[Y_{pq}pq + Y_{qr}qr] + \frac{\rho}{2}L^3[Y_p up + Y_r ur + Y_{vq}vq + Y_{wp}wp + Y_{wr}wr] +$$

$$\frac{\rho}{2}L^2[Y_v uv + Y_{vw}vw + Y_{\delta r}u^2\delta r] - \frac{\rho}{2}\int_{x_{tall}}^{x_{nose}}[C_{dy}h(x)(v + xr)^2 + C_{dz}b(x)(w - xq)^2] \cdot \frac{(v + xr)}{U_{cf}(x)}dx - \tag{4}$$

$$m[ur + x_G pq + z_G qr - wp - y_G(p^2 + q^2)] + (W - B)\cos\theta\sin\varphi$$

$$f_3(x,\mu) = \frac{\rho}{2} L^4 [Z_{pp} p^2 + Z_{pr} pr + Z_{rr} r^2] + \frac{\rho}{2} L^3 [Z_q uq + Z_{vp} vp + Z_{vr} vr] +$$

$$\frac{\rho}{2} L^2 [Z_w uw + Z_{vv} v^2 + u^2 (Z_{\delta s} \delta_s + u^2 (Z_{\delta s} \delta_s + Z_{\delta b} \delta_b))] +$$

$$\frac{\rho}{2} \int_{x_{tall}}^{x_{nose}} [C_{dy} h(x)(v+xr)^2 + C_{dz} b(x)(w-xq)^2] \cdot \frac{(w-xq)}{U_{cf}(x)} dx -$$

$$m[-uq + vp + x_G pr - y_G qr - z_G(p^2+q^2)] + (W-B)\cos\theta\cos\varphi$$

(5)

$$f_4(x,\mu) = \frac{\rho}{2} L^5 [K_{pq} pq + K_{qr} qr] + \frac{\rho}{2} L^4 [K_p up + K_r ur + K_{vq} vq + K_{vq} vq + K_{wp} wp + K_{wr} wr] +$$

$$\frac{\rho}{2} L^3 [K_v uv + K_{vw} vw] + (y_G W - y_B B)\cos\theta\cos\varphi - (z_G W - z_B B)\cos\theta\sin\varphi -$$

$$[y_G(-up+vp) - z_G(ur-wp)] - (I_z - I_y)qr - I_{xy}pr + I_{yz}(q^2+r^2) + I_{xz}pq$$

$$f_5(x,\mu) = \frac{\rho}{2} L^5 [M_{pp} p^2 + M_{pr} pr + M_{rr} r^2] + \frac{\rho}{2} L^4 [M_{uq} uq + M_{vp} vp + M_{vr} vr] +$$

$$\frac{\rho}{2} L^3 [M_{uw} uw + M_{vv} v^2 + u^2 (M_{\delta s} \delta s + M_{\delta b} \delta b)] -$$

(6)

$$\frac{\rho}{2} \int_{x_{tall}}^{x_{nose}} [C_{dy} h(x)(v+xr)^2 + C_{dz} b(x)(w-xq)^2] \cdot \frac{(w-xq)}{U_{cf}(x)} x dx -$$

$$(x_G W - x_B B)\cos\theta\cos\varphi - (z_G W - z_B B)\sin\theta - (I_x - I_z)pr + I_{xy}qr - I_{yz}pq - I_{xz}(p^2-r^2) +$$

$$m[x_G(-uq+vp) - z_G(-vr+wq)]$$

$$f_5(x,\mu) = \frac{\rho}{2} L^5 [M_{pp} p^2 + M_{pr} pr + M_{rr} r^2] + \frac{\rho}{2} L^4 [M_{uq} uq + M_{vp} vp + M_{vr} vr] +$$

$$\frac{\rho}{2} L^3 [M_{uw} uw + M_{vv} v^2 + u^2 (M_{\delta s} \delta s + M_{\delta b} \delta b)] -$$

$$\frac{\rho}{2} \int_{x_{tall}}^{x_{nose}} [C_{dy} h(x)(v+xr)^2 + C_{dz} b(x)(w-xq)^2] \cdot \frac{(w-xq)}{U_{cf}(x)} x dx -$$

(7)

$$(x_G W - x_B B)\cos\theta\cos\varphi - (z_G W - z_B B)\sin\theta - (I_x - I_z)pr + I_{xy}qr - I_{yz}pq - I_{xz}(p^2-r^2) +$$

$$m[x_G(-uq+vp) - z_G(-vr+wq)]$$

$$f_6(x,\mu) = \frac{\rho}{2} L^5 [N_{pq} pq + N_{qr} qr] + \frac{\rho}{2} L^4 [N_p up + N_r ur + N_{vq} vq + N_{wp} wp + N_{wr} wr] +$$

$$\frac{\rho}{2} L^3 [N_v uv + N_{vw} vw + N_{\delta r} u^2 \delta r] - \frac{\rho}{2} \int_{x_{tall}}^{x_{nose}} [C_{dy} h(x)(v+xr)^2 + C_{dz} b(x)(w-xq)^2] \cdot \frac{(v+xr)}{U_{cf}(x)} x dx +$$ (8)

$$m[x_G(ur-wp) - y_G(-vr+wq)]$$

$$f_7(x,\mu) = p + \dot{\psi}\sin\theta$$ (9)

$$f_8(x,\mu) = q - \dot{\psi}\sin\varphi\cos\theta$$ (10)

$$f_9(x,\mu) = r - \dot{\psi}\cos\varphi\cos\theta$$ (11)

In the equation φ is heeling angle, θ is trim angle, W is gravity, B is buoyancy, the significance of the other symbols and the magnitude of the values refer to the literature [13]. State variable is $x=[u,v,w,p,q,r,\phi,\theta,\psi]$, forking parameter is

$$\mu=[\delta_r,\delta_b,\delta_s,\delta_B,x_{GB},y_{GB},r_{GB}], \quad \delta_B=B-W \text{ and } \delta_B\in[-20\%B,20\%B].$$

3. Submarine turning performance simulation experiment

In this experiment, Computational Fluid Dynamics (CFD) simulation [14] is utilized to simulate the flow field around the SUBOFF submarine as it turns. The simulation generates data on the flow around the hull during the turning maneuver. Additionally, a comparison is made between the flow fields around the submarine at various deflection angles.

In this experiment, the turning motion of SUBOFF submarine in the horizontal plane is simulated, and considering the stability of the hull itself and other issues, only its motion in the horizontal plane (transverse swings, longitudinal swings, and bow swings) is considered, and the motion in the vertical plane (transverse swings, longitudinal swings, and pendant swings) is constrained. By adjusting the rudder angle of the vertical rudder, the SUBOFF submarine is calculated for self-propelled turning, the results of its turning trajectory, forces and moments, and other characteristics are analyzed.

3.1 Determination of self-propelled points

In the field of ship or submarine design and performance analysis, the "point of self-propulsion" is a key concept that refers to a state in which the thrust generated by the propeller is balanced by the drag encountered by the hull under certain conditions. In this state, the submarine is able to sail at a constant speed without the need for additional thrust to overcome the drag. This state of equilibrium is critical to the maneuverability and energy efficiency of the submarine. In this study, specific parameters from the self-point-of-voyage state were used in exploring the submarine turning performance to ensure accuracy and relevance of the analysis. The specific self-navigation point data are shown in the table below.

**Table 1. Specific parameters of the self-propelled point of rotation of the submarine in this paper**

Characteristics	Numerical value
Speed	2.75m/s
Propeller speed	607.70rpm
Push, resistance	92.068N

3.2 Grid division and calculation of working conditions

3.2.1 Grid division

The mesh type used in the calculation of turning motion is hexahedral mesh for the submarine attached structure encrypted and unencrypted two cases of mesh delineation, in the process of hull turning, the wake current is not always parallel to the hull of the X-axis

direction, but presents a circular arc, so in the wake current encrypted area of the shape is changed into the form of the bend, see Figure 2, so that the wake current motion can be described more clearly and the direction of the vertical rudder corresponds to the direction of the wake current encrypted. The direction of vertical rudder corresponds to the direction of wake encryption.
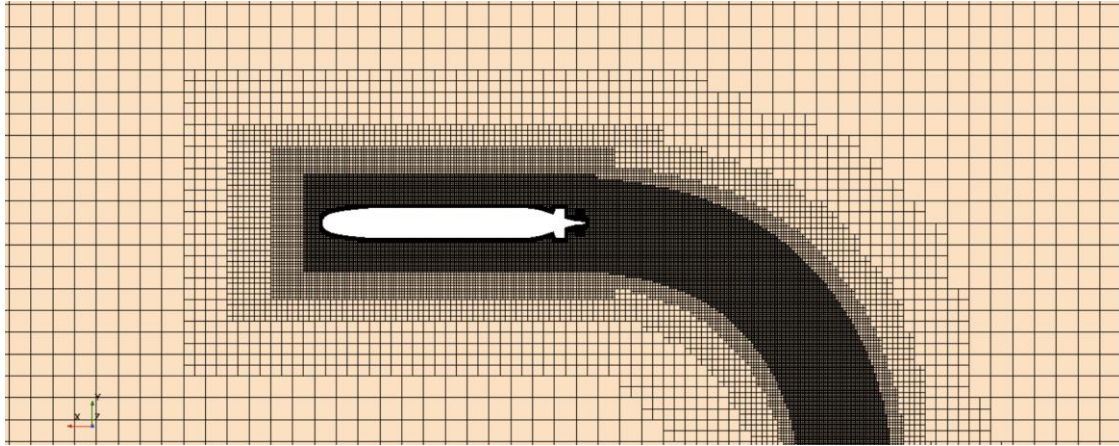

Figure. 2. Meshing of rotary motion

3.2.2 Calculation of working conditions

In this paper, the cross rudder is used to complete the calculation of the turning motion, adjusting the rudder angles of different vertical rudders and keeping the rudder angle of the horizontal rudder unchanged, in which the positive and negative directions of the rudder angle are specified based on the turning direction of the hull, and the rudder angle is positive when the hull is rotated clockwise in the horizontal plane in accordance with the law of right-handed helix as shown in Fig. 3. A total of six rudder angles are selected for calculation, which are -6°/6°, -12°/12° and -18°/18°, among which the rudder angle of -6°/6° is shown in Fig. 4.
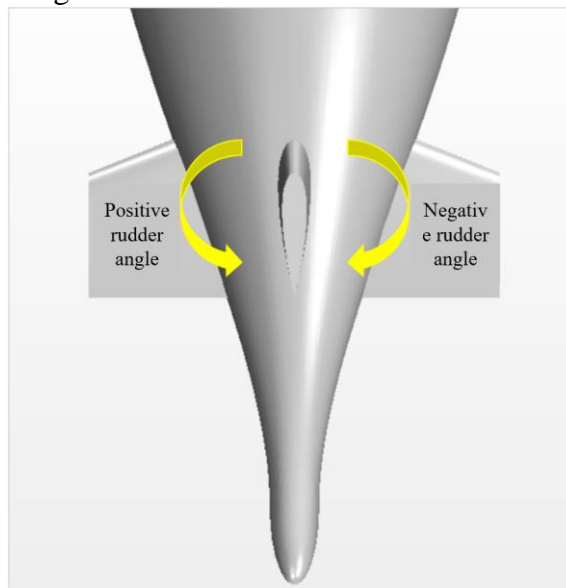
Figure. 3. Schematic diagram of rudder angle direction

(a)   Rudder

angle 6°
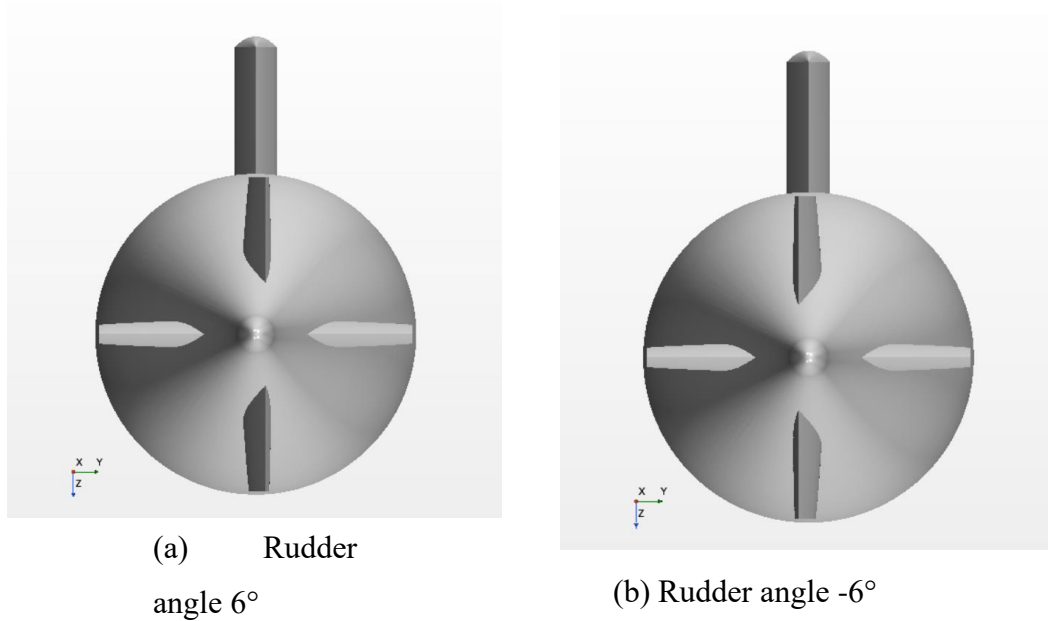
(b) Rudder angle -6°
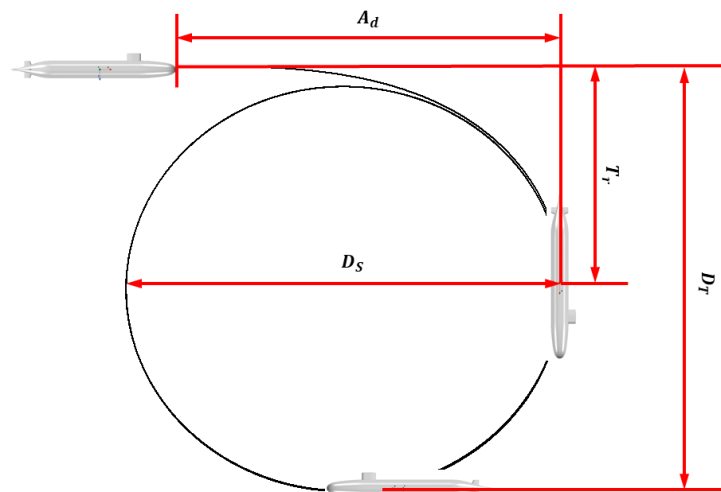
Figure. 4. Schematic diagram of -6°/6° rudder angle

3.3 Turning motion calculation results

3.3.1 Turning characteristic parameter analysis

The turning motion is based on the SUBOFF submarine's self-propelled point for the prediction calculation, similar to the dynamic prediction above, the DFBI (Dynamic fluid body interaction)model [15] is used, the propeller speed is 617.36 rpm, and the hull accelerates to the self-propelled point from the zero speed, and then it starts to turn the rudder until the completion of the turning motion, in order to reduce the computation time, when setting up the DFBI model, the hull's initial speed is set to 2.75 m/ s, and let it start to turn the rudder directly from the self-heading point.

According to the characteristic features of the turning motion, the main characteristic parameters are classified into constant turning diameter D_S, tactical diameter D_T, longitudinal distance A_d, positive transverse distance T_r, airspeed V_s、 of constant turning, drift angle β_s, turning period T, etc., see Fig. 5.

Figure. 5. Schematic diagram of characteristic parameters of rotation

The turning process of SUBOFF hull with 12° rudder angle is shown in Fig. 6, and it can be clearly seen that the wake flow is in the shape of a circle, and it takes about 25s to turn 360°, and the simulation time in this paper will make the hull complete at least 2 circles of turning. The rotary trajectory of the center of gravity of the boat under different rudder angles is shown in Fig. 7, which keeps a straight line at the initial stage, then bends, and finally becomes a circle, the x-axis of the SUBOFF follower coordinate system is the center of gravity of the boat pointing to the bow of the boat, and the y-axis is the center of gravity of the boat pointing to the starboard side, and the boat is rotated to the right when the rudder angle is positive and to the left when the rudder angle is negative, and the radius of the rotary is decreasing with the increase of rudder angle, and the trajectory of the first circle has deviations from the second circle at the initial stage of rotation, and the rest has deviations from the initial stage of the second circle. The trajectories of the first circle are basically coincident except for the deviation from the second circle in the initial stage of turning, and the second circle starts to enter the constant turning stage. In the case of negative rudder angle, the constant rotary diameters D_S corresponding to -6°, -12°, and -18° rudder angles are $3.82L_{PP}$, $2.93L_{PP}$, and $2.44L_{PP}$, respectively; on the contrary, in the case of positive rudder angle, the constant rotary diameters D_S corresponding to +6°, +12°, and +18° rudder angles are $3.76L_{PP}$, $2.91L_{PP}$, $2.32L_{PP}$.
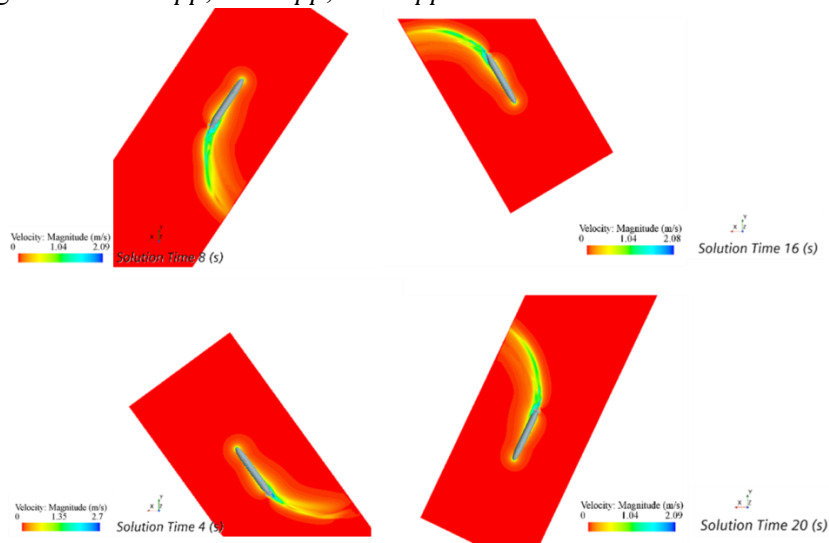

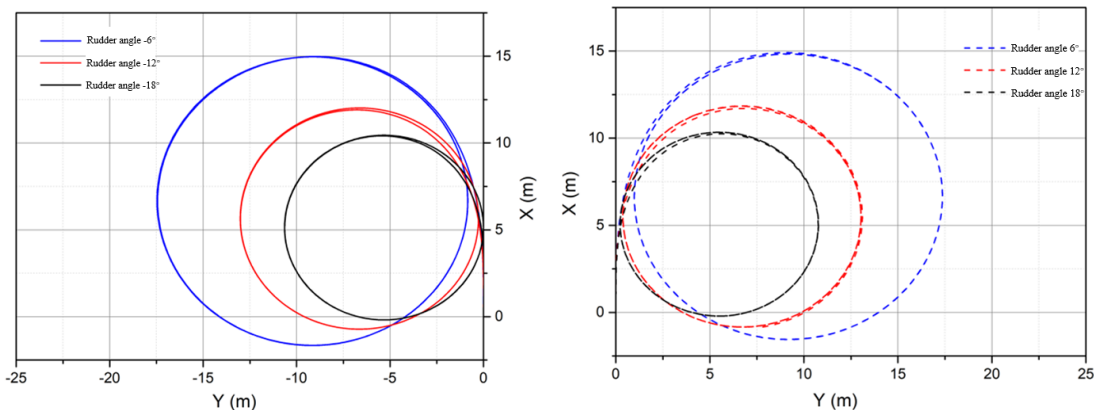**Figure. 6. Hull turning process with 12° rudder angle**

Figure. 7. Hull rotation trajectory under different rudder angles

In the turning process, the turning speed under different rudder angles is shown in Fig. 8, with the change of time, the hull speed decreases gradually, roughly 15s later, the acceleration is close to zero, and the speed begins to stabilize, this process is called speed drop, this is due to the hull in the process of turning the rudder turning process, the hull and rudder are subject to the resistance as well as the flow to the propeller of the fluid are changed, at this time the propeller is in the oblique navigation of the flow field, part of the thrust force At this time, the propeller is in the flow field of oblique navigation, part of the thrust force is consumed in the process of centripetal acceleration change, the larger the rudder angle is, the smaller the final stabilized speed is, i.e., the more obvious the phenomenon of speed drop is, the turning speeds under the rudder angles of -6°/6°, -12°/12°, and -18°/18° are reduced by about 37.45%, 45.45%, and 51.27%, respectively.
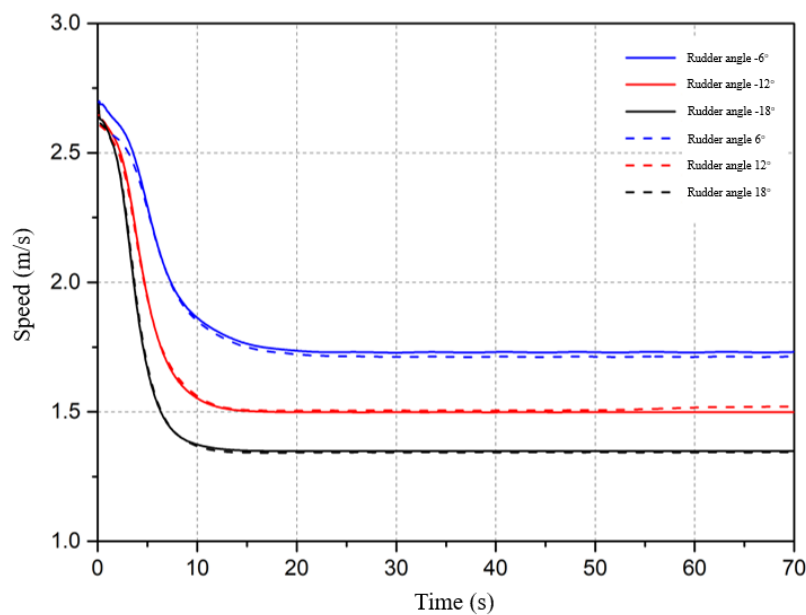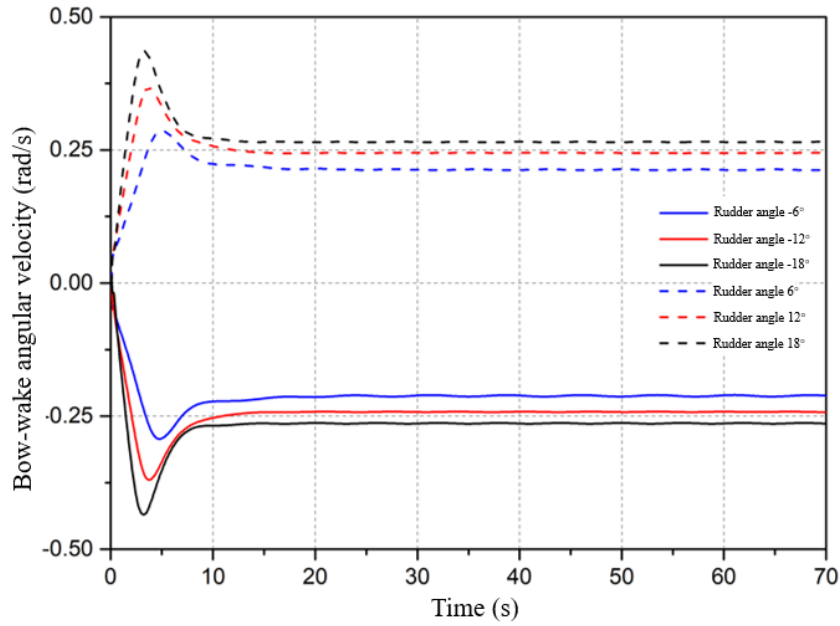

Figure. 8. Hull rotation speed under different rudder angles

The time history curves of drift angle and bow rocking angle velocity under different rudder angles are shown in Fig. 9. and Fig. 10., which can be seen that the trends of these two changes are similar, reaching a peak value in about 4~5s, then changing in the reverse direction and reaching a stable value in about 20s. The reason for the peak value is that, due to the submarine's inertia, the submarine cannot generate a large bow rocking angle velocity in time in the initial stage after rudder maneuvering, and under the action of lateral force, a transverse movement velocity is generated, which forces the weight of the boat to move in the direction opposite to that of rudder generation, called "reverse traverse". Instead, under the action of the lateral force, a transverse speed is generated, forcing the center of the boat to move in the direction opposite to the direction of the rudder generated, which is called "reverse transverse shift". Positive rudder angle and negative rudder angle have little effect on the drift angle and bow rocking speed, only change the direction of these two, and the drift angle and bow rocking speed both increase with the increase of rudder angle, the rest of the characteristic parameters are shown in Table 2.
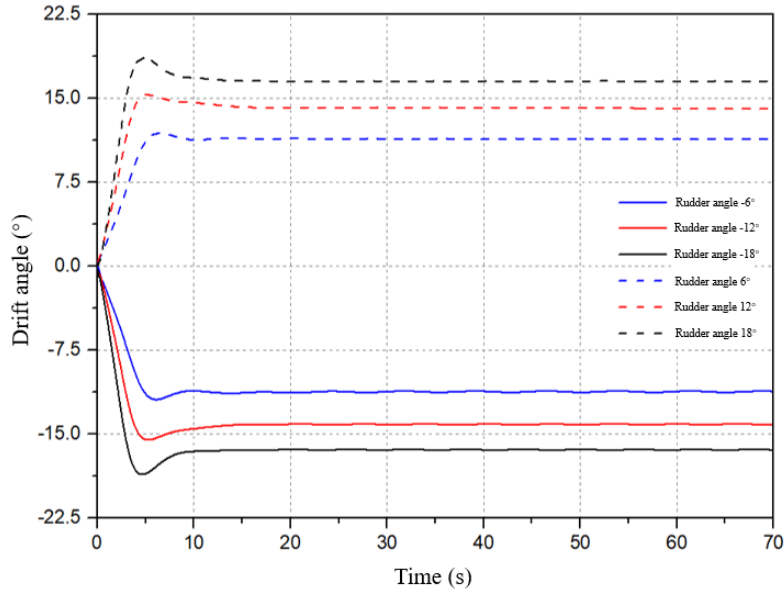
Figure. 9. Hull rotation drift angle under different rudder angles

Figure. 10. Hull yaw angular velocity under different rudder angles

Table 2. Characteristic parameters of hull rotation under different rudder angles

Parameterization	flat	Rudder angle					
		-6°	-12°	-18°	6°	12°	18°
Steady turning diameter D_S	m	16.62	12.74	10.64	16.38	12.66	10.11
Tactical diameter D_T	m	17.29	12.83	10.42	17.22	12.85	10.56
Longitudinal spacing A_d	m	14.82	11.71	10.17	14.77	11.52	10.01
Measuring line T_r	m	7.36	5.20	3.87	7.53	5.32	4.09

|							
Steady turning speed V_s	m	1.73	1.50	1.35	1.71	1.52	1.34
Drift angle β_s	°	-11.16	-14.12	-16.38	11.35	14.07	16.54
Heading angle velocity ω	rad/s	-0.21	-0.24	-0.26	0.21	0.24	0.27
Turning period T	s	29.20	24.80	22.56	29.20	24.64	22.24

3.3.2 Force and moment analysis

Figure 11(a) and Figure 11(b) show the time history images of thrust and drag during the turning process of the SUBOFF submarine. Thrust increases with time, rapidly so in the first 0~10 seconds. Drag initially peaks and then decreases during the early stages of the turn, with both forces stabilizing after 20 seconds. The greater the rudder angle, under the same propeller rotational speed, the greater the axial thrust generated. The thrust forces corresponding to rudder angles of -6°/6°, -12°/12°, and -18°/18° are approximately 125N, 137N, and 146N, respectively. In contrast, the hull's resistance is less affected by the rudder angle, with resistance values stabilizing around 75N. It can be observed that at this time, the propeller's thrust force and the hull's resistance are not equal. This discrepancy is because, during the turning process, the propeller's thrust force must overcome not only the axial resistance of the hull but also the axial drag force. Additionally, it must provide the necessary force to maintain stability. It is also important to note that the propeller's thrust force is used to counteract the hull's lateral force during the turn.

Figure 12 shows the time history images of propeller torque under different rudder angles. The change trend is similar to the thrust curve described previously. The propeller torque increases with the increase of the rudder angle and shows a significant upward trend around 5 seconds. This increase occurs because the hull's turning motion completes its initial stage at this time. The reverse displacement ends, the bow moves towards the turning circle, and the turning angular velocity gradually stabilizes.

(a) Thrust   (b) Resistances
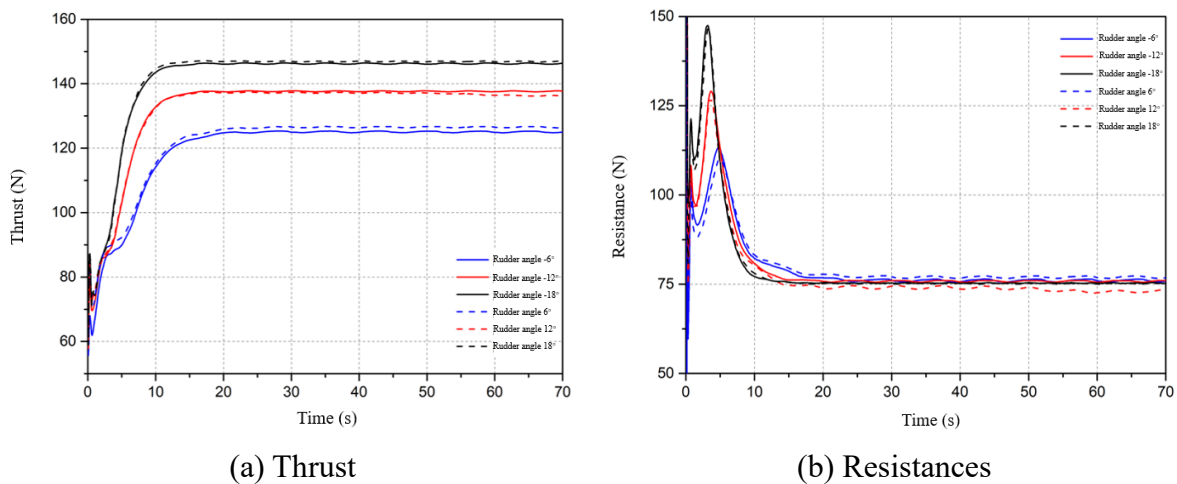
Figure. 11. Thrust and drag time history curves under different rudder angles
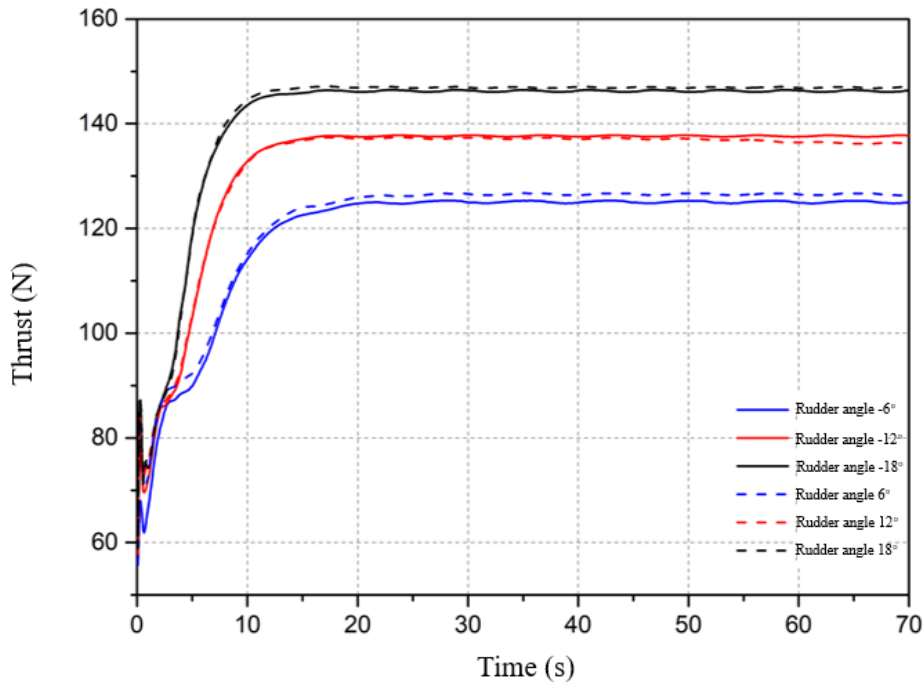
Figure. 12. Time history curve of propeller torque under different rudder angles

The rudder and hull lateral force under different rudder angles are shown in Figs. 13 and 14, both exhibiting a similar trend. Initially, they increase and then gradually decrease to stabilization. The hull experiences a lateral force of approximately 250N. Positive and negative rudder angles correspond to opposite directions of the lateral force, with equal magnitudes. In Fig. 13, it can be observed that the rudder lateral force peaks around 5 seconds. The larger the final rudder angle, the greater the lateral force on the rudder. This is because as the rudder angle increases, the sinusoidal value of the angle between the rudder and the hull's Gy-axis decreases. Consequently, when rudders with different angles are subjected to the same hydrodynamic force, the one with a smaller angle will distribute more of this force to the Gy-axis as a lateral force. This, combined with the lateral forces from other attachments and the hull itself, provides the centripetal force necessary for the turning motion.
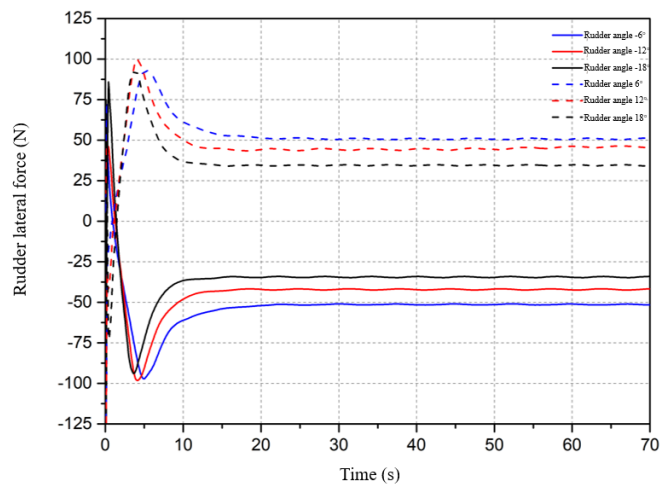

Figure. 13. Time history curve of tail rudder lateral force under different rudder
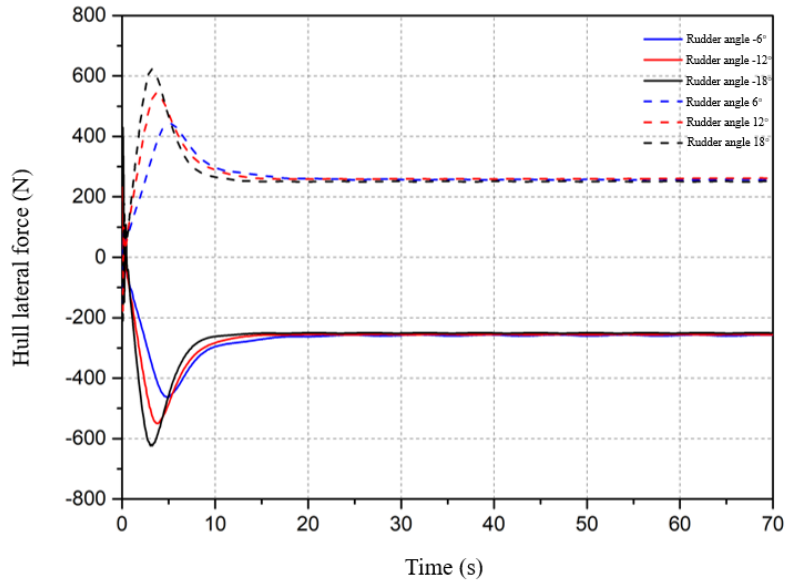
angles

Figure. 14. Time history curve of hull lateral force under different rudder angles

Table 3 and Figure 15 reflect the lateral forces in different parts of the hull. It can be seen that most of the lateral forces are generated by the bare hull without any attachments, accounting for about 72% of the total. The vertical rudder and the command deck contribute to 19% and 8% of the total forces, respectively. Additionally, the horizontal rudder generates lateral forces that are all less than 1N.
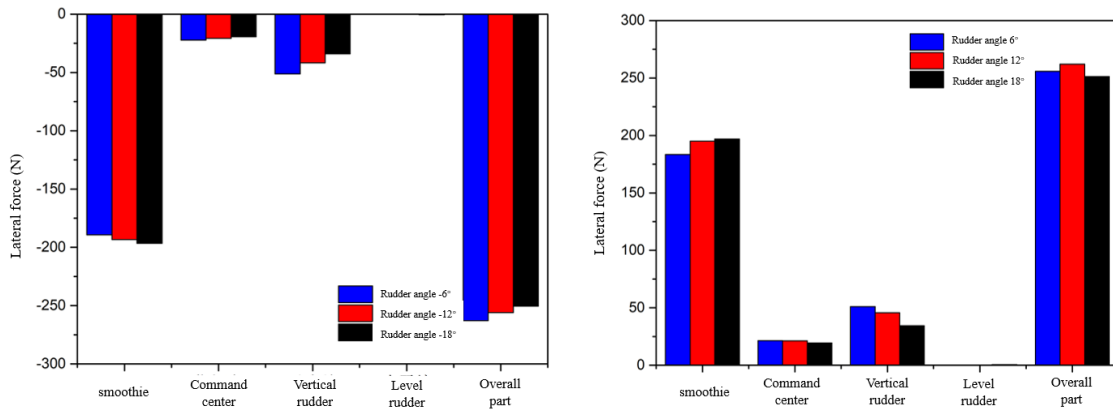
Figure. 15. Lateral forces at different parts of the hull under different rudder angles

**Table 3. Lateral forces at different parts of the hull**

Position	Flat	Rudder angle					
		-6°	**-12°**	**-18°**	**6°**	**12°**	**18°**
Light bulb		-189.32	-193.43	-196.61	183.47	195.00	196.95
Command center		-22.19	-20.68	-19.36	21.51	21.19	19.40
Vertical rudder	N	-51.17	-41.73	-34.04	51.13	45.61	34.38
Horizontal rudder		-0.28	-0.25	-0.51	-0.26	0.22	0.59

| Population | -262.96 | -256.09 | -250.52 | 255.85 | 262.02 | 251.32 |

3.3.3 Flow field analysis

From the above, it is concluded that positive and negative rudder angles have a slight effect on the force exerted on the hull during the turning motion. However, the turning trajectory and characteristic parameters are essentially similar, and the overall effect is not pronounced. The following analysis of the pressure and velocity fields will use only the positive rudder angle as an example. Figure 16 shows the pressure distribution on the hull's surface under rudder angles ranging from 6° to 18°. It is observed that the pressure on the left side of the hull (i.e., the outer side of the turning circle) is significantly higher than that on the right side. The pressure difference between the two sides reaches a maximum at the hull's one-third point, which then provides sufficient lateral force for the hull's turning motion.

Figure 17 shows the rudder pressure distribution corresponding to different rudder angles. It can be observed that the pressure distribution in the horizontal rudder area is approximately symmetrical. There is a noticeable negative pressure area on the right side of the vertical rudder, while the left side is a positive pressure area. This indicates that the rudder force is directed from the left side to the right side. (The terms "left" and "right" are defined from the perspective of the stern looking towards the bow of the boat.) The pressure differential provides a certain sideways force that aids in the turning motion.

Rudder angle 6°
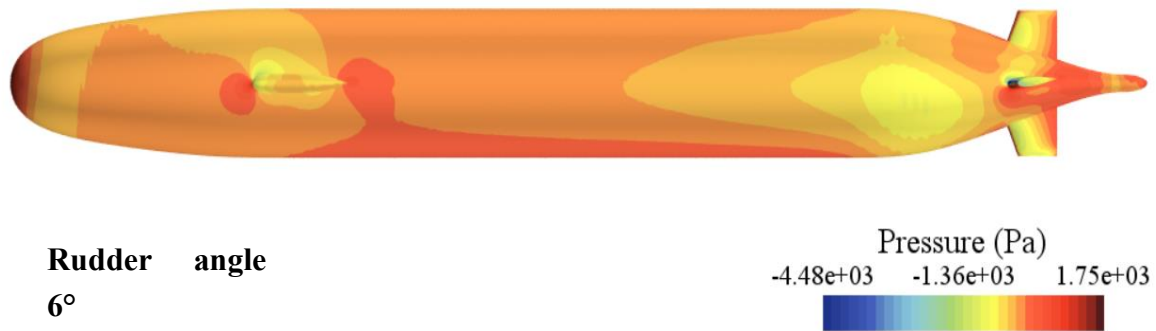
(a) Rudder angle 6°

Rudder angle 12°

(b) Rudder angle 12°

Rudder angle 18°

(c) Rudder angle 18°

Figure. 16. Hull pressure field corresponding to 6°, 12° and 18° rudder angles
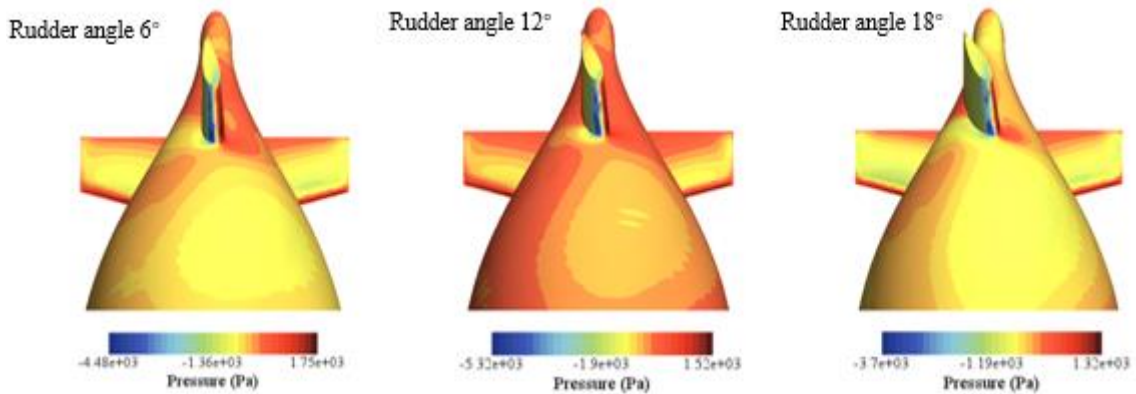

Figure. 17. Tail rudder pressure field corresponding to 6°, 12° and 18° rudder angles

Figure 18 shows the velocity flow field in the mid-longitudinal section corresponding to rudder angles of 6° to 18°. The shape of the flow field around the hull is similar, with differences in velocities at various positions on the hull's surface. The velocity at the stern is greater than that at the bow. There is no obvious velocity stratification between the hull's inlet section and the junction of the parallel mid-body with the surrounding fluid. However, the velocity around the hull's rear is higher as it is farther from the bow. The distribution of velocities is essentially symmetrical about the xGy plane. This is attributed to the presence of a propeller drive at the stern, which results in higher velocities in the region close to the stern.
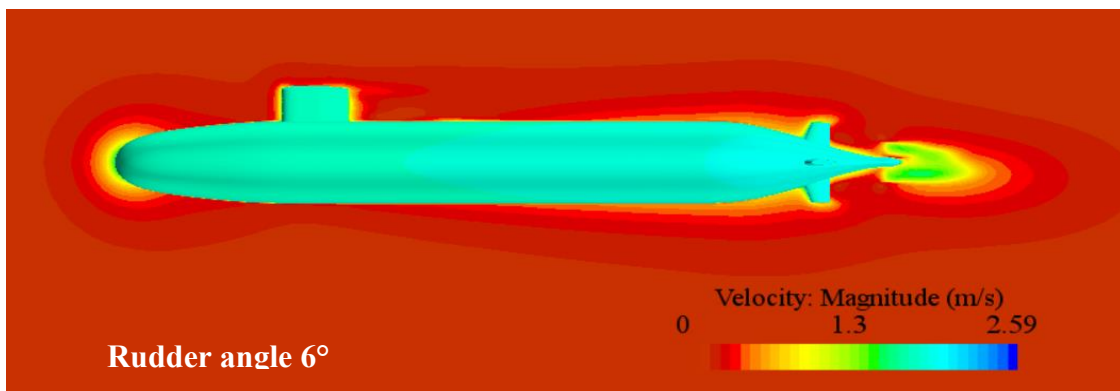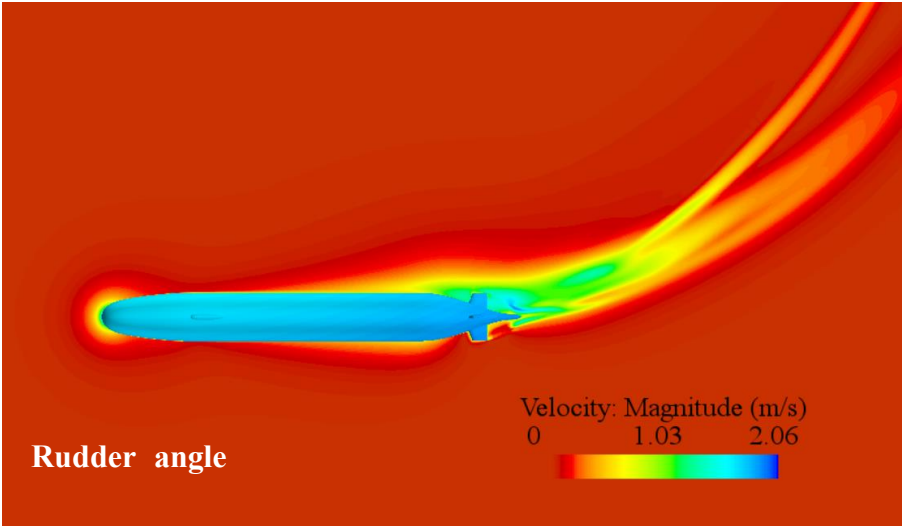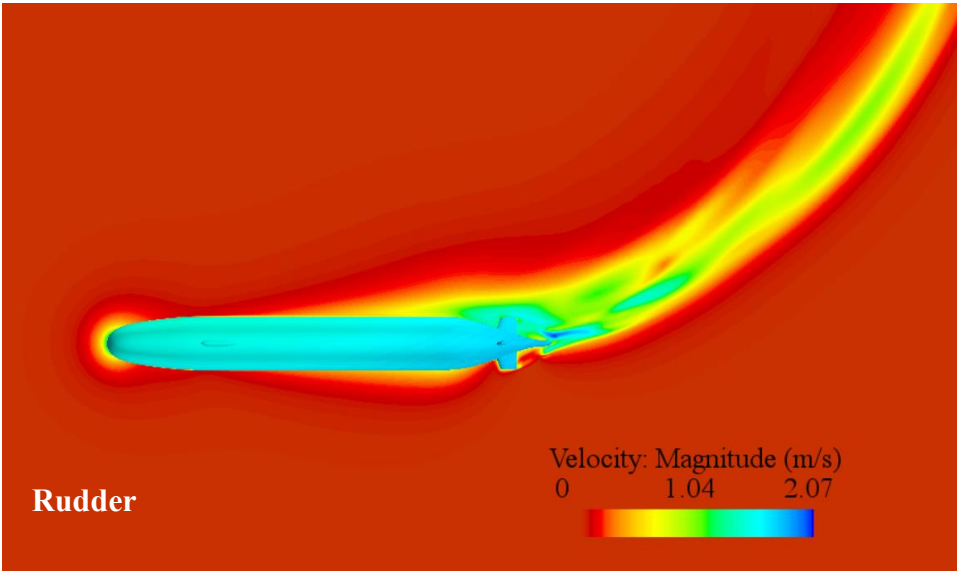

Rudder angle 6°

(a) Rudder angle 6°
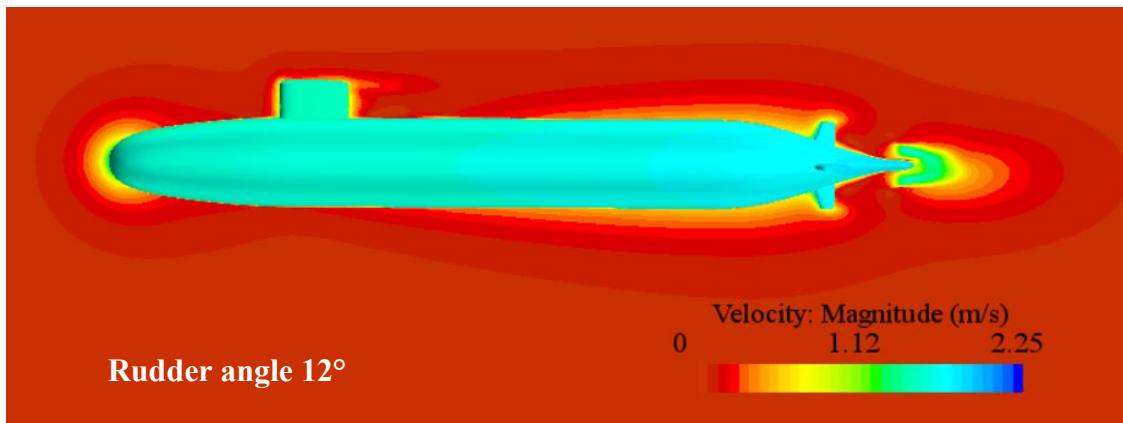
(b) Rudder angle 12°
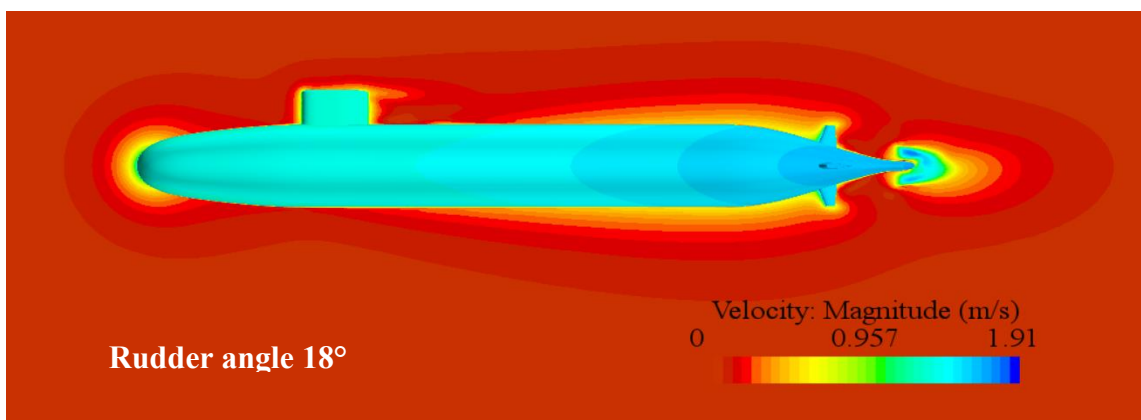
(c) Rudder angle 18°

Figure. 18. Velocity nephogram corresponding to different rudder angles (middle longitudinal section)

To more accurately describe the flow field during the hull's turning, the velocity field in the horizontal plane under various rudder angles is calculated. The velocity fields corresponding to rudder angles of 6°, 12°, and 18° are depicted in Fig. 19. The wake flow field exhibits a distinct arc shape, and the velocity distribution around the hull is similar to that observed in Fig. 18. A bifurcation phenomenon is observed in the wake field at the 6° rudder angle. The wake flow near the center of the turn is influenced by the vertical rudder, while the remainder is affected by the hull's own rotation. The main reason for the bifurcation phenomenon is that the angle between the hull's rotation speed and the Gx axis (the drift angle) is smaller than the angle of the vertical rudder. As the rudder angle increases, the wake area expands, indicating a superposition of the vertical rudder's wake field with that of the hull. The drift angle and the rudder angle become increasingly similar. The numerical relationship between these angles is detailed in Table 4.

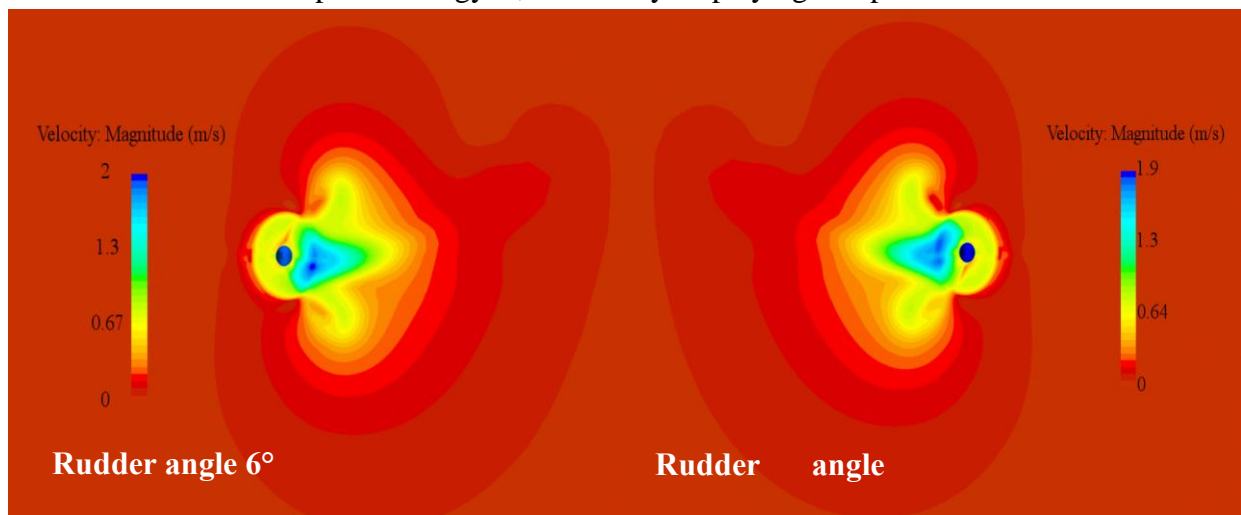(a) Rudder angle 6°

(b) Rudder angle 12°
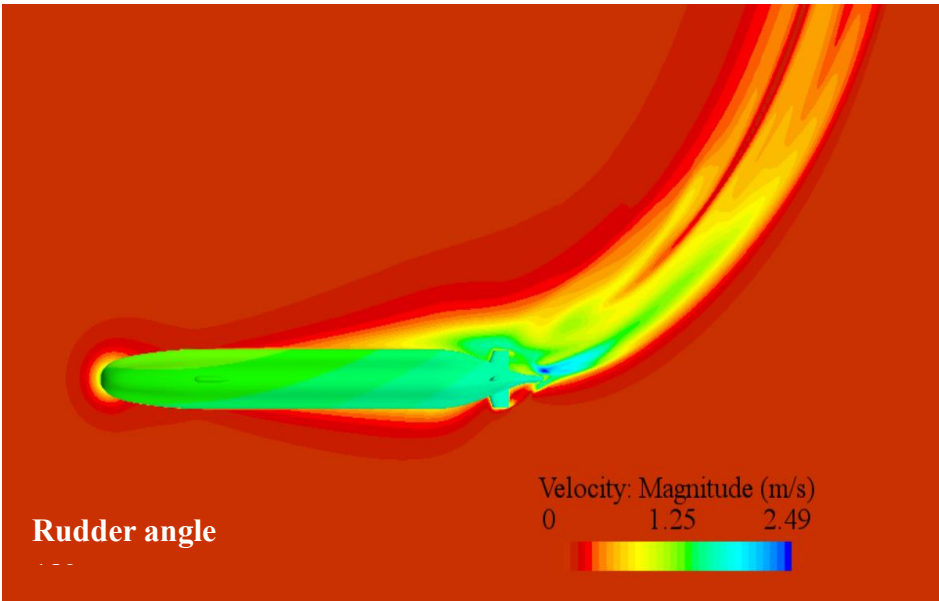
(c) Rudder angle 18°

Figure. 19. Velocity nephogram diagram corresponding to different rudder angles (horizontal plane)

Table 4. Comparison results of vertical rudder angle and drift angle

| Rudder angle	Drift angle	Relative difference (absolute value)
-6°	-11.16°	5.16°
-12°	-14.12°	2.12°
-18°	-16.38°	1.62°
6°	11.35°	5.35°
12°	14.07°	2.07°
18°	16.54°	1.46°

The velocity distribution at the paddle disk surface under different rudder angles is depicted in Fig. 20. It is evident that the propeller rotation generates a circular velocity field, with the highest velocities observed around the inner area of the rotary circle near the propeller. The velocity field in the surrounding area exhibits a petal-like shape, influenced by both the vertical and horizontal rudders. As the rudder angle increases, the petal shape becomes increasingly indistinct. The velocity distribution around the upper and lower vertical rudders is not symmetrical, primarily due to the commanding station's impact on the flow field. The flow fields generated by the rudder and the commanding station intermingle around the propeller. Notably, only the lower vertical rudder beneath the hull significantly influences the surrounding flow field. Using the 12° rudder angle as an example, Fig. 21 illustrates the velocity flow field at various longitudinal positions of the hull. It can be observed that the command deck's influence on the flow field progressively shifts towards the inner part of the gybe, eventually displaying an upward trend.

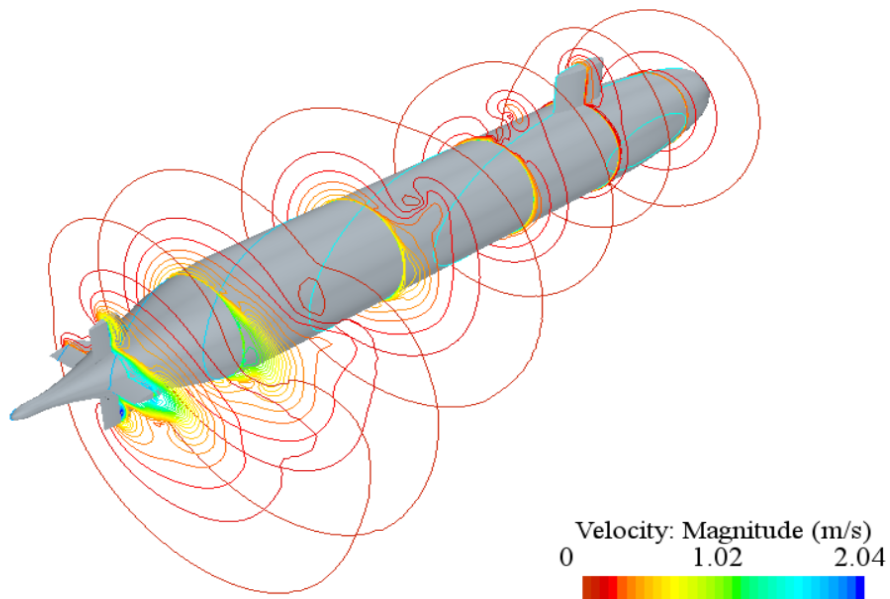Rudder angle 6°   Rudder   angle
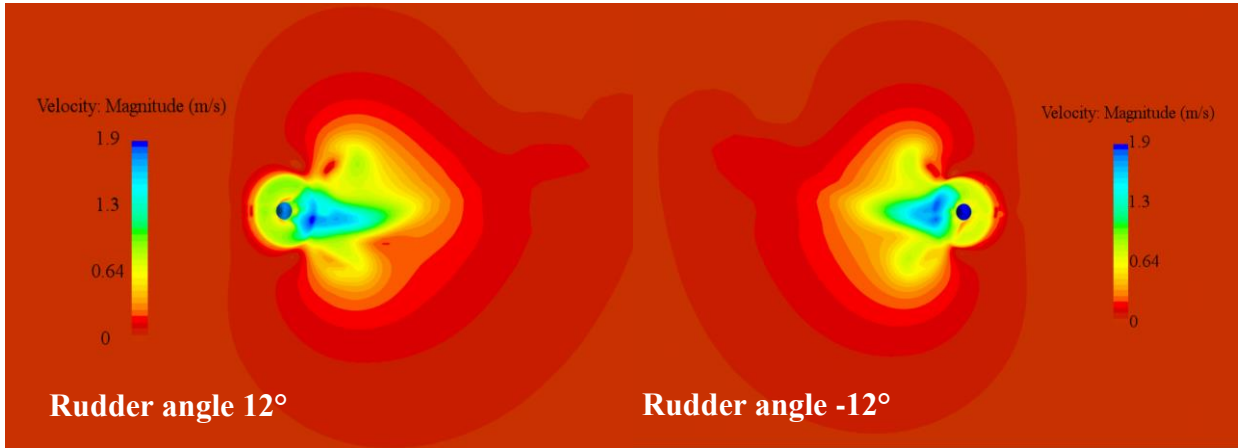
(a) Rudder angle -6°/6°

(b) Rudder angle -12°/12°
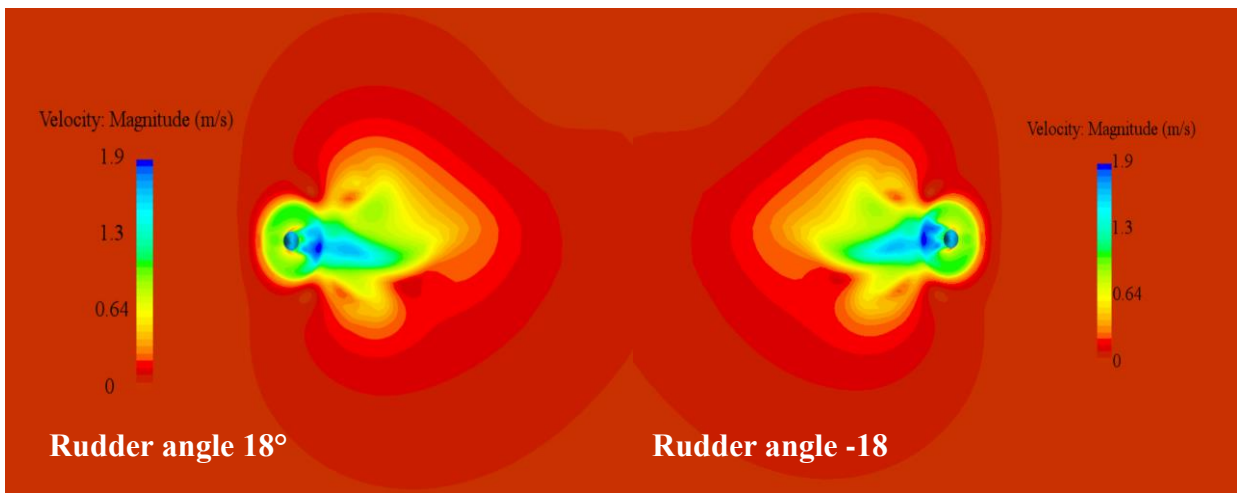
(c) Rudder angle -18°/18°

Figure. 20. Velocity nephogram diagram corresponding to different rudder angles (propeller disk surface)

Figure. 21. Velocity field at different positions of the hull corresponding to 12° rudder angle

4 Conclusion

In this paper, a simulation experiment is conducted at a speed of 2.75 m/s. The DFBI model is employed for predicting the turning of the SUBOFF submarine under six rudder angles: -6°/6°, -12°/12°, and -18°/18°. The simulation considers only the three-degree-of-freedom motion within the horizontal plane. The turning characteristic parameters, forces, and flow field conditions under these different rudder angles are calculated and analyzed.

In terms of turning speed, changes in the resistance of the hull and the flow of water to the propeller lead to the phenomenon known as "speed drop" [16]. The final speed is reduced by approximately 30% to 50%. The larger the rudder angle, the more pronounced this speed drop phenomenon becomes.

The trends of drift angle, bow rocking speed, and lateral force with time are similar. All of these parameters peak during the initial stage of turning and then decrease to a stable value during the constant turning stage. Positive and negative rudder angles have minimal impact on the drift angle and bow rocking speed, primarily affecting their direction. Both the drift angle and bow rocking speed increase with larger rudder angles. In terms of lateral force, it is found to be directly proportional to the rudder angle. Calculating the lateral force on different parts of the hull reveals that the lightweight body without attachments generates the largest proportion of lateral force. This is followed by contributions from the vertical rudder and the command deck.

The pressure distribution diagram of the hull clearly shows the pressure difference between its left and right sides. This pressure difference reaches a maximum at one-third of the hull's length, providing sufficient lateral force for turning. In the wake region, the smaller the rudder angle, the larger the relative difference between it and the hull's drift angle, resulting in a more pronounced bifurcation phenomenon of the wake. Additionally, the influence of the command deck on the flow field at different longitudinal positions along the hull gradually shifts to the inner side of the turning circle, ultimately showing an upward trend. Moreover, the larger the rudder angle, the more the rudder's influence on the velocity field at the paddle plate surface is skewed towards the horizontal plane.

4 Summarize

In response to the challenges encountered in the experiment, we propose a series of practical improvement measures to ensure the overall enhancement of the submarine's performance. Firstly, we will focus on optimizing the rudder angle adjustment strategy by introducing an adaptive control system. This system will enable real-time, precise adjustment of the rudder angle, significantly reducing the speed drop phenomenon and enhancing the submarine's stability.Additionally, we suggest the following enhancements:

1. Hull Design: Streamline optimization and the incorporation of adjustable parts will be pursued to bolster the maneuverability and response speed of the submarine. These improvements will better equip the submarine to navigate complex water environments effectively.

2. Propeller Performance: We will develop high-efficiency propellers and explore variable pitch designs to adapt to diverse operating conditions. By improving propulsion efficiency and responsiveness, the submarine's overall performance will be heightened.

3. Application of Flow Field Control Technology: Advanced technologies such as micro-jets or flow control surfaces will be employed to refine the flow field around the hull. This approach aims to reduce fluid resistance, thereby enhancing the submarine's overall performance.

4. Management of Lateral Force: Optimization of the rudder and hull structure will facilitate effective distribution and regulation of lateral force. By reducing reliance on a single rudder or structure, these enhancements will bolster the submarine's maneuverability and safety.

These measures collectively aim to address key performance limitations and elevate the submarine's effectiveness in various operational scenarios.

Conflict of interest: The authors of the article have consulted with each other and have no conflict of interest.

References:

1. Till, Geoffrey. "Maritime strategy and the twenty-first century." The Journal of Strategic Studies 17.1 (1994): 176-199.
2. WU, Ziyin, et al. "RESEARCH STATUS AND PROSPECT OF SONAR DETECTING TECHNIQUES NEAR SUBMARINE   ." Advances in Earth Science 20.11 (2005): 1210.
3. Vego, Milan. "The Role of the Attack Submarines in Soviet Naval Theory." Naval War College Review 36.6 (1983): 48-64.
4. Bakos, George K., and James N. Eagle. Submarine approach and attack tactics: simulation and analysis. Diss. Naval Postgraduate School, 1995.
5. Zhang, Y., Xie, Y., Zhao, G., Liang, Z., Shi, J.,and Yang, Y. "The Important Role of Fluid Mechanics in the Engineering Field." Mechanics 9 (1977): 421-445.
6. Y. Zhang, D. Zhang, Y. Zhang, Y. Xie, B. xie, H. Jiang, A Comprehensive Review of Simulation Software and Experiemntal Modeling on Exploring Marine Collision Analysis, ENG Transactions 4 (2023) 1–7.
7. Zhang, D., Zhao, B., Zhang, Y., and Zhou, N. "Numerical simulation of hydrodynamics of ocean-observation-used remotely operated vehicle." Frontiers in Marine Science 11 (2024): 1357144.

8. Zhang, Yi, Dapeng Zhang, and Haoyu Jiang. "Review of Challenges and Opportunities in Turbulence Modeling: A Comparative Analysis of Data-Driven Machine Learning Approaches." Journal of Marine Science and Engineering 11.7 (2023): 1440.

9. Liu Qinxian, Zhu Genxing, Lu Wei. Modeling and simulation of submarine turning motion. Computer Measurement and Control 01(2003):62-63+77. (in Chinese)

10. He Guangxing, et al. Numerical simulation of internal and external rudder horizontal plane turning maneuvering in X-rudder submarines. Ship Engineering 45.09(2023):53-60. d (in Chinese)

11. Li SQ, Ye JM, and Zhang HK. Characterization of underwater fixed-depth turning of submarines with X rudder and cross rudder. Ship Mechanics 24.11(2020):1433-1442.(in Chinese)

12. Sato, Yohei, Hideaki Miyata, and Toru Sato. "CFD simulation of 3-dimensional motion of a ship in waves: application to an advancing ship in regular heading waves." Journal of marine science and technology 4 (1999): 108-116.

13. Healey, Anthony J., and David Lienard. "Multivariable sliding mode control for autonomous diving and steering of unmanned underwater vehicles." IEEE journal of Oceanic Engineering 18.3 (1993): 327-339.

14. Zoontjes, Richard, Harm Siegersma, and Harald Ottens. "Using CFD to determine heave added mass and damping of a suction pile." International Conference on Offshore Mechanics and Arctic Engineering. Vol. 43451. 2009.

15. Takahashi, Kenshiro, and Prasanta K. Sahoo. "Fundamental CFD study on the hydrodynamic performance of the DARPA SUBOFF submarine." International Conference on Offshore Mechanics and Arctic Engineering. Vol. 58776. American Society of Mechanical Engineers, 2019.

16. Feng, Dakui, et al. "Comparisons of turning abilities of submarine with different rudder configurations." International Conference on Offshore Mechanics and Arctic Engineering. Vol. 51265. American Society of Mechanical Engineers, 2018.